Journal of
Applied Crystallography

ISSN 0021-8898

Received 15 August 2006
Accepted 30 January 2007

On the heterogeneous character of water's amorphous polymorphism

Michael Marek Koza,* Roland P. May and Helmut Schober

Institut Laue Langevin, 6 rue Jules Horowitz, F-38042 Grenoble, France. Correspondence e-mail: koza@ill.fr

In this paper we report *in situ* small-angle neutron scattering results on the high-density amorphous (HDA) and low-density amorphous (LDA) ice structures and on intermediate structures as found during the temperature-induced transformation of HDA into LDA. We show that the small-angle signal is characterized by two Q regimes featuring different properties [Q is the modulus of the scattering vector defined as $Q = (4\pi/\lambda_i)\sin(\theta)$ with θ being half the scattering angle and λ_i the incident neutron wavelength]. The very low Q regime ($< \sim 5 \times 10^{-2}$ Å^{-1}) is dominated by a Porod-limit scattering. Its intensity reduces during the course of the HDA-to-LDA transformation following kinetics reminiscent of those observed in wide-angle diffraction experiments. The small-angle neutron scattering form factor in the intermediate regime of $5 \times 10^{-2} < Q < 0.5$ Å^{-1} for HDA and LDA features a rather flat plateau. However, the HDA signal shows an ascending intensity towards smaller Q marking this amorphous structure as heterogeneous. When following the HDA-to-LDA transition, the form factor shows a pronounced transient excess in intensity marking all intermediate structures as strongly heterogeneous on a length scale of some nanometres.

1. Introduction

Throughout recent years different concepts have been introduced to explain the phenomenon of amorphous polymorphism, *i.e.* the existence of more than one amorphous structure in a single substance (Mishima & Stanley, 1998; Stanley *et al.*, 2000; Debenedetti, 2003). The most intriguing scenario is based on the existence of two distinct liquid states, which was established as a possibility in molecular dynamics simulations (Poole *et al.*, 1993). The liquid polymorphism was supposed to account for the formation of the high-density amorphous (HDA, $\rho \simeq 39$ molecules nm^{-3}) and the low-density amorphous (LDA, $\rho \simeq 31$ molecules nm^{-3}) ice structures as the quenched liquid phases. This scenario has been successfully extended towards other systems, indicating that amorphous polymorphism, as a manifestation of distinct liquid states, could be a general feature of condensed matter (Kurita & Tanaka, 2004, 2005). However, it has been equally questioned by recent computer experiments that introduced a band of transformation scenarios spanning between the extrema of a pure relaxation phenomenon of an amorphous matrix and a multiple-phase transition scheme (Guillot & Guissani, 2003; Brovchenko *et al.*, 2003; Martonak *et al.*, 2004).

Obtaining experimental proof of or evidence against the two-liquid scenario in water is a subtle task, as any attempt to directly access the hypothetical two-liquid regime is bound to fail. Fingerprints of liquid polymorphism, thus, are looked for in the amorphous states. One crucial indicator is the presence of a first-order transition between HDA and LDA. However, any experimental approach towards a classification of the HDA-to-LDA transformation is severely hampered by the non-ergodic nature of the amorphous structures (Koza, Geil, Schober & Natali, 2005).

Hence, an experimental search for characteristic features that might help to discern between the proposed thermodynamic concepts is the only approach to shedding some light on the origin of the amorphous polymorphism of ice. One characteristic feature of the HDA-to-LDA transformation is an enhancement of the elastic signal in the small-angle scattering regime. The very first *in situ* studies of the HDA-to-LDA transformation have already shown that despite the continuously changing static and dynamic structure factors of the amorphous ice there is also a transient excess signal at low scattering angles (Schober *et al.*, 1998, 2000). The enhanced small-angle neutron scattering (SANS) and small-angle X-ray scattering (SAXS) signals could be understood as the response of frozen-in density variations, *i.e.* spatial heterogeneities, occurring transiently during the structural transformation of HDA into LDA.

In this paper we report *in situ* neutron diffraction experiments in the small-angle scattering regime monitoring structures of typically 10–1000 Å. From a set of time- and temperature-dependent experiments, we are able to substantiate the transient, thoroughly heterogeneous character of the intermediate transition stages on a spatial scale of some nanometres and to describe qualitatively the temperature dependence and time evolution of the transient heterogeneities. We will equally show that beyond the Q regime of the transient enhanced scattering there is a signal due to interfaces whose kinetics follow the wide-angle response (Koza *et al.*, 2003).

2. Experimental

All samples were prepared by slow compression of D_2O (purity 99.8%) ice I_h at $T \simeq 77$ K up to pressures of 1.8 GPa in a piston cylinder apparatus (Koza *et al.*, 2003). Each preparation run resulted in a sample volume of 3 ml. To meet the condition of a 10% scattering sample for the suppression of multiple scattering, the samples were carefully crushed into millimetre-sized chunks and placed within a

cadmium diaphragm into a standard flat aluminium sample holder. The diaphragm optimized the size of the sample, leaving a free space 12 mm in diameter and about 2.2 mm thickness at its centre with respect to the homogeneous neutron beam.

The purity of the HDA samples had been confirmed at the spectrometer IN6 ($0.3 \leq Q \leq 2.7$ Å^{-1}) before they were mounted for measurements in a standard cryostat at the small-angle diffractometer D22. Q is the modulus of the scattering vector defined as $Q = (4\pi/\lambda_i)\sin(\theta)$ with θ and λ_i being half the scattering angle and the wavelength of the incident radiation, respectively. Both instruments are situated at the Institut Laue Langevin in Grenoble, France. The transmissions of the samples were determined experimentally in the HDA state at D22 to 89 ± 2% corresponding to an effective sample thickness of 1.5 ± 0.3 mm. Samples had been kept for about 30 min at 78 K for complete removal of liquid nitrogen before any high-accuracy measurement was started. During the experiments an atmosphere of 200 mbar of helium was applied.

The measurements were carried out with an incident neutron wavelength of 6 Å and additional test measurements were carried out with a wavelength of 24 Å in order to access the largest structural units. A lowest limit of $Q \simeq 5 \times 10^{-4}$ Å^{-1} could be reached. The exploitation of such a large Q range in practice requires modification of the instrumental setup. High-accuracy measurements in the structurally stable states HDA and LDA were carried out with three detector-to-sample distances, namely 1.4, 5 and 18 m. The data-acquisition time was 10 min at each position. The setup choice for *in situ* studies of the transforming structures was contingent upon the transformation kinetics at the chosen temperatures since a dead time of 1.72 min was due to the setup changes. Consecutive measurements were performed with a detector-to-sample distance of 1.4 and 10 m for 3 min each. At 105 K only a single detector-to-sample distance of 2.5 m could be used due to the fast transformation kinetics of the sample.

In this paper we can only present a subset of our experimental data. The four samples reported here were followed *in situ* at the nominal temperatures of 100, 101.5, 103 and 105 K. Please note that throughout this paper we refer to the sample states measured prior to the heat treatment as HDA and those after the transformation and an annealing procedure at 127 K as LDA. No changes of the LDA structure factor could be found upon cooling of the samples back to ~78 K.

Standard data corrections for the empty can and background scattering were applied for the detector-to-sample distances 1.4, 2.5, 5 and 10 m. The calibration of the detector and normalization to absolute units were accomplished with a water (H_2O) standard of 0.1 mm thickness. The effective scattering power of the water standard at λ = 6 Å was taken into account (Lindner & Zemb, 2002). All corrections and the azimuthal averaging of the two-dimensional data were done with the software package *GRASP* (Dewhurst, 2002). For clear presentation, the data sets were normalized to unity with respect to an LDA baseline. The normalization factor onto an absolute scale is $4.8\,(1) \times 10^{-2}$ cm^{-1}.

3. Results

3.1. Static properties of HDA and LDA

For the readers' convenience we report in Fig. 1 a selected set of wide-angle diffraction (WAD) data recorded during the HDA-to-LDA transformation at the diffractometer D20 at the Institut Laue Langevin. The grey-shaded area picks out the small-Q regime in which intensity changes indicate that the sample passes through a state of strongest heterogeneity (SSH). Note that the HDA structure already displays an intensity higher than that of LDA, which is in agreement with previous neutron and X-ray scattering studies (Schober *et al.*, 1998, 2000; Koza, Geil, Winkel *et al.*, 2005; Koza *et al.*, 2006). The small-Q signal of the other intermediate tranformation stages has been suppressed for clarity.

Small-angle scattering data collected at D22 are shown in Fig. 2. In the left panel we report the intensities of all samples measured in the HDA and the LDA states. The data sets for different samples have been shifted for clarity. Two features dominate the signal: an apparently flat background at $Q > 5 \times 10^{-2}$ Å^{-1}, comprising contributions from the incoherent scattering from D_2O and from density variations that can be associated with the compressibility of the amorphous matrix, and a power-law scattering towards smaller Q. The pronounced power-law dependence $S(Q) \propto Q^{-4}$ is the so-called Porod-limit scattering (PLS). It is the final slope of a SANS form factor that appears due to a sharp boundary between two phases in a sample and depends only on the scattering contrast and the interface area, but not on the shape of the structures or particles present in the sample (Glatter & Kratky, 1982; Lindner & Zemb, 2002). Note that the intensity of the PLS was well reproduced in all our samples following the same preparational procedure. At low Q, our data do not cover the range necessary to observe a Guinier-limit scattering. Furthermore, comparison of results obtained with 6 and 24 Å show a clear influence of multiple scattering on the data (Lindner & Zemb, 2002). The intensities of the PLS were determined to be

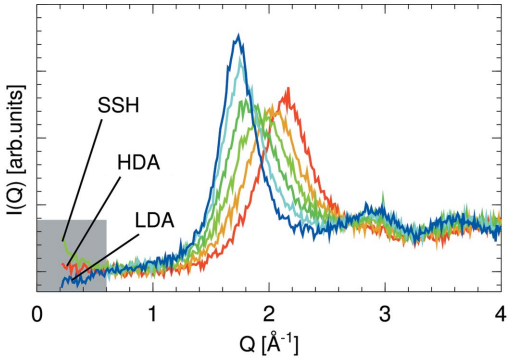

Figure 1
Diffraction data recorded during the course of the HDA-to-LDA transformation. The small-Q intensity indicates a transient intensity excess and a state of strongest heterogeneity (SSH) can be identified.

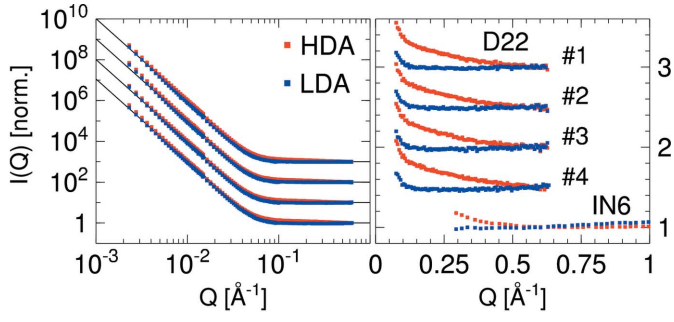

Figure 2
Left: SANS intensity $I(Q)$ of four different samples in the HDA and LDA sample states. The data have been shifted for clarity. Solid lines represent fits to the data with a PLS and a constant background fixed to unity as described in §2. Right: a close-up of $I(Q)$ in the intermediate Q range. Also shown is the signal recorded on IN6 and reported by Schober *et al.* (1998). The data have been shifted for clarity.

$4.8\,(1) \times 10^{-15}$ and $3.7\,(1) \times 10^{-15}$ Å^{-1} for HDA and LDA, respectively. Please see the Appendix for more information.

Let us focus in the following on the momentum range $Q > 0.1$ Å^{-1}, *i.e.*, on the apparently flat background beyond the PLS. The right panel of Fig. 2 reports the intensities of the four samples compared to prior results obtained on the spectrometer IN6 (Schober *et al.*, 1998). As has been shown before in X-ray and neutron scattering experiments (Schober *et al.*, 1998, 2000; Koza, Geil, Winkel *et al.*, 2005; Koza *et al.*, 2006), an excess of the SAS signal indicates a pronounced heterogeneous character of the initial HDA structure. In contrast, the LDA modification shows a constant signal. These features are entirely reproducible.

3.2. Transformation from HDA to LDA

Fig. 3 reports the *in situ* SANS form factors $I(Q, t, T)$ of sample 2 (left-hand side) and 1 (right-hand side) in a double-log plot. As indicated by the vertical arrows, the increase of the transient signal is plotted in the top figures and its downturn is shown in the bottom figures. The time t after which the data were recorded is also shown.

It is evident that $I(Q, t, T)$ in the SANS regime presented here is a characteristic measure of the HDA-to-LDA transition. In analogy to the features of the WAD signal described by Koza, Geil, Schober & Natali (2005), we can find for any $I(Q, t, T = 103\,\mathrm{K})$ a matching signal observed at a different T after a well defined but different evolution time t. As a consequence, it is not only the mere presence of a SANS signal that is characteristic of the intermediate structures, but it is in particular its intensity and the details of its profile that discern and, basically, define distinct transition stages.

A similarity with the WAD signal can be also found in the kinetic properties computed from $I(Q, t, T)$. For simplicity we restrict our consideration here to intensities integrated over two different Q ranges. One range ($10^{-2} \leq Q \leq 2 \times 10^{-2}$ Å^{-1}) stresses the PLS evolution [$I_P(t, T)$] and the other ($0.1 \leq Q \leq 0.15$ Å^{-1}) represents the Q regime of the transient excess scattering [$I_I(t, T)$]. Fig. 4 shows the time dependence of $I_P(t, T)$ (top panel) and $I_I(t, T)$ (bottom panel) of the two samples. The data have been normalized as described by Koza, Geil, Winkel *et al.* (2005). $I_P(t, T)$ takes on values between unity, representing the HDA state, and null, representing the LDA state. $I_I(t, T)$ is defined as null for the LDA state and unity for the SSH. Note that the poor statistics of the $I_P(t, T = 105\,\mathrm{K})$ signal is due to the limited Q range given by the detector-to-sample distance of 2.5 m.

$I_P(t, T)$ displays a dependence well comparable with the evolution of the WAD signal reported in detail by Koza *et al.* (2003). Two features dominate the time response. First, a sluggish transformation process is observable, and then a sigmoid-shaped (Avrami–Kolmogorov-type) step is detectable. Although $I_P(t, T)$ bears the fingerprints of an Avrami–Kolmogorov-type transformation, the entire process cannot be understood as a simple nucleation and growth scenario (Doremus, 1985). This has been discussed in detail by Koza *et al.* (2003).

We may find a simple explanation for the equivalent behaviour of the PLS and WAD kinetics. Taking into account the fact that the intensity of the PLS is proportional to the square of the difference in scattering density and the specific surface $\Delta\rho^2 \sim S/V$, it is an index of the density of the sample. In an equivalent way a dependence has been established between the density of amorphous samples and the relative position of the structure factor maximum determined by structural changes on a local length scale of some ångstroms (Elliott, 1991, 1995).

It has been indicated recently based on diffraction experiments (Koza, Geil, Winkel *et al.*, 2005) that the kinetics of the SANS signal in the intermediate Q range is also closely related to the WAD. Here we show that this relation applies as well to the PLS kinetics. The SSH can always be found close to the centre of the transformation between HDA and LDA. This behaviour is independent of T. However, one has to take some care when interpreting $I_I(t, T)$ in detail. The decisive and accurate observable constitutes the Porod-invariant $q = \int_0^\infty I_h(Q)Q^2\,\mathrm{d}Q$ of the form factor $I_h(Q)$ which characterizes exclusively the transient excess scattering. This form factor is dwarfed by the PLS intensity towards smaller Q. Nevertheless, a relation between the SSH position and the centre of the transformation has been unequivocally established in all our experiments accessing the intermediate Q range and either the PLS or the WAD signals.

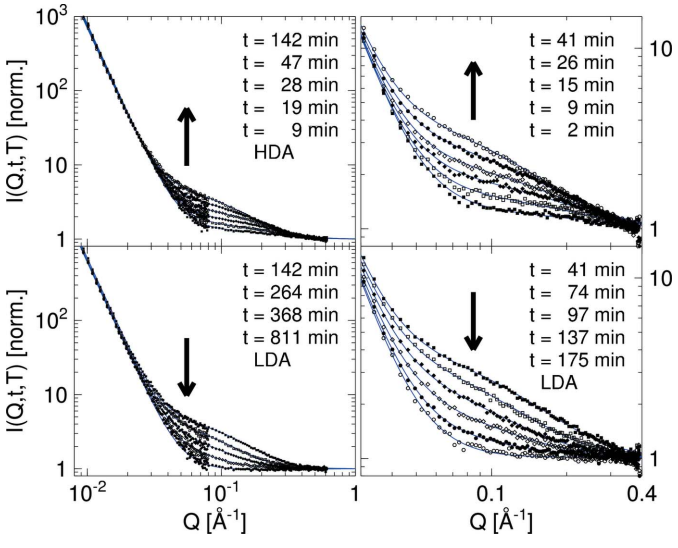

Figure 3
Left: Intensity evolution $I(Q, t, T = 103\,\mathrm{K})$ measured at different stages of the HDA-to-LDA transformation for sample 2. As indicated by the vertical arrows, the top figure reports the increase of the transient signal and the bottom figure shows its downturn. The time t after which the signal was recorded is indicated. Solid lines are guides to the eye. Right: the corresponding signal evolution measured for sample 1 at 105 K.

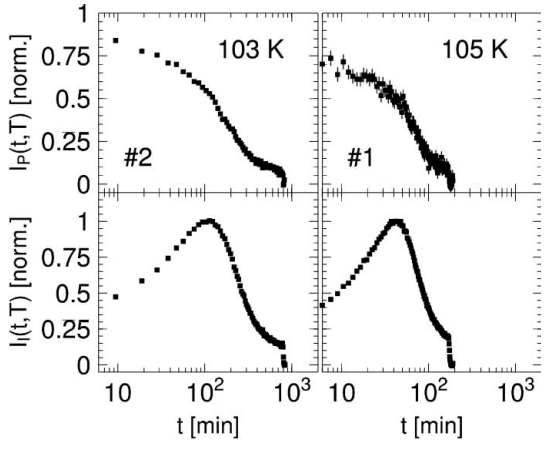

Figure 4
Left: Kinetic response of sample 2 in the Porod-limit scattering $I_P(t, T = 103\,\mathrm{K})$ and the intermediate Q regime $I_I(t, T = 103\,\mathrm{K})$. Right: Corresponding response of sample 1 at 105 K. Please note that the fall of the signals at the end of the data sets is due to the annealing process of the samples to LDA at 127 K.

4. Discussion

The present SANS data establish unequivocally the thoroughly heterogeneous nature of the amorphous ice structures when following the transformation from HDA to LDA. These characteristics exclude the possibility of a homogeneous relaxation process of an amorphous ice matrix. Hence, to explain the transformation behaviour we may think of two other simple scenarios.

First, taking the non-ergodicity of the amorphous ice structures into consideration, we may think of the sample as being composed of sub-ensembles each of which is governed by distinctly different relaxation dynamics, *i.e.* relaxing for a given T on different timescales. This heterogeneity in relaxation behaviour translates into a strong spatial heterogeneity of the system while going through the transition, the reason being the large density differences between the still present high-density and already relaxed low-density sub-ensembles.

Second, a first-order transition may not be excluded as a process underlying the HDA-to-LDA transformation. Since this transformation is accompanied by an appreciable density change of almost 30%, the kinetics of the transformation are expected to be strongly perturbed by the additional elastic energy contribution, as discussed by Tanaka (2000). In particular, we may expect that early transition stages encountering molecules within a low-density environment surrounded by a high-density matrix will be strongly stressed. On a local scale, the sample is influenced by a non-uniform pressure distribution leading to departures from the properties of a non-stressed bulk low-density amorphous structure.

Irrespective of the scenario, *i.e.* a heterogeneous relaxation or a real phase transition, underlying the transformation between a high-density and a low-density amorphous structure, it is obvious that HDA as prepared by compression at 77 K is a heterogeneous structure on a nanometre scale. Hence, it is tempting to consider the very high density amorphous ice modification as the initial stage of the transformation (Mishima, 1996; Loerting *et al.*, 2001; Koza, Geil, Winkel *et al.*, 2005; Koza *et al.*, 2006). As a consequence, the heterogeneous character of HDA has to be properly accounted for when structural properties are computed or modelled in real space from experimental data. The pronounced small-angle signal should in general be a help in discerning between different models trying to explain the phenomenon of amorphous polymorphism.

The overall behaviour reported here for amorphous ice modifications is not unlike the properties reported for a different system showing apparently amorphous polymorphism, namely triphenylphosphite (TPP). A thoroughly heterogeneous character for the TPP sample passing through a phase transition between two homogeneous states has been established by nuclear magnetic resonance, light scattering and SANS experiments (Senker *et al.*, 2005). TPP SANS data show a pronounced PLS and an excess signal at intermediate Q in the amorphous state (Alba-Simionesco & Tarjus, 2000). Light-scattering data confirm the transient heterogeneous nature of the sample on a micrometre scale and indicate complex kinetics of the transition which can deviate from an Avrami–Kolmogorov nucleation and growth scenario when the transition happens *via* a spinodal decomposition (Kurita & Tanaka, 2004). Moreover, the properties of the intermediate stages cannot be reproduced by a superposition of the properties of the initial and the final transition states, *i.e.* the superposition principle fails.

The features established during the spinodal decomposition in TPP signify the complexity of a transition between amorphous structures, which might equally be the case for amorphous ice. This finding forces us to conclude that superposition principles, isosbestic point criteria or classical nucleation and growth scenarios are of no particular significance when trying to account for the real origin and nature of the transformation between amorphous ice structures.

5. Conclusion

We have used SANS techniques to study the structural properties of amorphous ice modifications on mesoscopic length scales. It has been shown that the HDA ice produced by compressing crystalline ice is a heterogeneous structure on a spatial scale of some nanometres. When following the transformation of HDA into the LDA modification, the SANS signal displays a contrast maximum at about the centre of the transformation. Thus, the sample passes through a state of strongest heterogeneity.

As has been reported earlier and is shown here in detail, the transient SANS signal is a characteristic feature of the HDA-to-LDA transformation, and it is intrinsic to structures intermediate with respect to the very high density amorphous (vHDA) modification and LDA.

When following the HDA-to-LDA transformation *in situ*, the evolution of the Porod-limit scattering shows a time dependence reminiscent of the WAD signal (Koza *et al.*, 2003). Its kinetics cannot be described by a pure Avrami–Kolmogorov time dependence that would characterize a plain nucleation and growth scenario. We have pointed out and discussed in detail the fact that the non-applicability of a nucleation and growth scenario does not exclude a real phase transition of first order between two amorphous ice structures. We may only draw the conclusion that a homogeneous relaxation of an amorphous matrix is to be excluded as a possible transformation scenario between high-density and low-density amorphous ice.

APPENDIX *A*
Porod-limit scattering

An obviously important question is the origin of the strong PLS in the samples. The PLS persists in the explored Q range and timescales of the experiments not only beyond their recrystallization to ice I_c (Koza, Geil, Schober & Natali, 2005; SANS data not shown here) but also upon annealing HDA into the very high density modification (Koza *et al.*, 2006). We tried to reduce the PLS intensity, *e.g.* by different sample treatments. For example, we measured HDA disc samples of about 1 mm thickness and 12 mm diameter before and after crushing them into millimetre-sized chunks. The sample consistency did not affect the PLS intensity appreciably. If we consider a scenario of uniform, spherically shaped heterogeneous domains as the source of the PLS and approximate the scattering densities by the sample-to-vacuum contrast, we may estimate the size of the domains as 1–10 μm. Hence, they are well separated by at least two orders of magnitude from the transient structural changes on the intermediate scale and sufficiently large to accommodate crystallites of ice I_c after a recrystallization of LDA.

The consistent reproducibility of the PLS indicates that it is either a generic feature of the amorphous ice samples or is created by the compression process of the crystalline ice matrix. For this reason we have examined crystalline samples that had been precompressed to different pressures. Fig. 5 reports example data from three different runs. The first crystalline sample was formed within the pressure device as for the preparation of the amorphous structure at 77 K, however, no pressure was applied. The second sample was precompressed to 0.9 GPa, which corresponds to a pressure close to the formation of HDA. Fig. 5(c) reports the signal measured with one of the HDA samples having been compressed to 1.8 GPa.

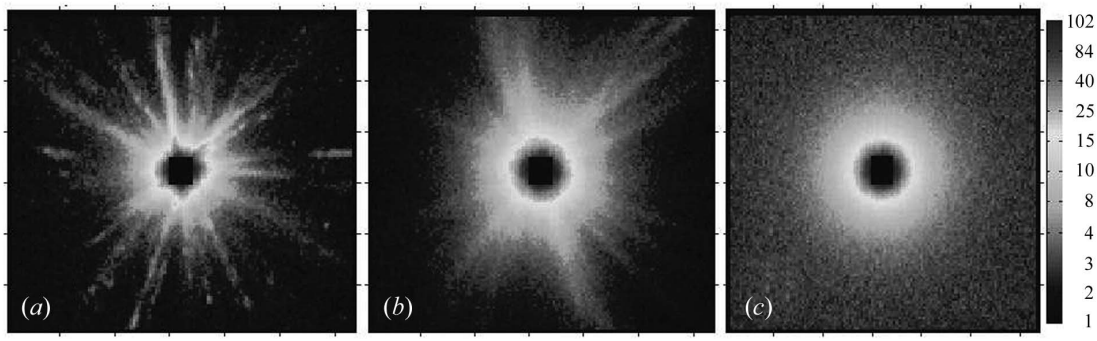

Figure 5
Contrast plot of the two-dimensional signal measured with three samples having been precompressed to 0 GPa (a), 0.9 GPa (b) and 1.8 GPa (c).

All our test runs showed a pronounced presence of impurities, dislocations and stacking faults already within the uncompressed crystalline samples. This is visualized in Fig. 5(a) by the anisotropic scattering features. On applying pressure to the samples, the signal from the perturbed crystalline matrices indicated a trend towards isotropic scattering (Fig. 5b) and completely isotropic features were reached in the HDA structures (Fig. 5c). Although this observation is based on *ex situ* compression runs, it indicates that the PLS is a generic feature of the compressed ice samples and might be of essential significance for the formation of the amorphous matrix. It is interesting and important to note that the pressure at which amorphous ice can be formed depends on the consistency and grain size of the initial sample state (Johari, 2000). The lowest formation pressure of HDA is observed when compressing the LDA matrix, *i.e.* when the PLS scattering gives evidence of a strong and isotropic distribution of interfaces within the amorphous matrix.

References

Alba-Simionesco, C. & Tarjus, G. (2000). *Europhys. Lett.* **52**, 297–303.
Brovchenko, I., Geiger, A. & Oleinikova, A. (2003). *J. Chem. Phys.* **118**, 9473–9476.
Debenedetti, P. G. (2003). *J. Phys. Condens. Matter*, **15**, R1669–R1726.
Dewhurst, C. (2002). *Graphical Reduction & Analysis SANS Program*. Institut Laue Langevin, Grenoble, France.
Doremus, R. H. (1985). *Rates of Phase Transitions*. London: Academic Press.
Elliott, S. R. (1991). *Phys. Rev. Lett.* **67**, 711–714.
Elliott, S. R. (1995). *J. Non-Cryst. Solids*, **182**, 40–48.
Glatter, O. & Kratky, O. (1982). *Small Angle X-ray Scattering*. London: Academic Press.
Guillot, B. & Guissani, Y. (2003). *J. Chem. Phys.* **119**, 11740–11752.
Johari, G. (2000). *Phys. Chem. Chem. Phys.* **2**, 1567–1577.
Koza, M. M., Schober, H., Fischer, H. E., Hansen, T. & Fujara, F. (2003). *J. Phys. Condens. Matter*, **15**, 321–332.
Koza, M. M., Geil, B., Schober, H. & Natali, F. (2005). *Phys. Chem. Chem. Phys.* **7**, 1423–1431.
Koza, M. M., Geil, B., Winkel, K., Köhler, C., Czeschka, F., Scheuermann, M., Schober, H. & Hansen, T. (2005). *Phys. Rev. Lett.* **94**, 125506-1–125506-4.
Koza, M. M., Hansen, T., May, R. P. & Schober, H. (2006). *J. Non-Cryst. Solids*, **352**, 4988–4993.
Kurita, R. & Tanaka, H. (2004). *Science*, **306**, 845–848.
Kurita, R. & Tanaka, H. (2005). *J. Phys. Condens. Matter*, **17**, L293–L302.
Lindner, P. & Zemb, T. (2002). *Neutron, X-Ray and Light Scattering*. Amsterdam: Elsevier Science Publishers BV.
Loerting, T., Salzmann, C., Kohl, I., Mayer, E. & Hallbrucker, A. (2001). *Phys. Chem. Chem. Phys.* **3**, 5355–5357.
Martonak, R., Donadio, D. & Parrinello, M. (2004). *Phys. Rev. Lett.* **92**, 225702-1–225702-4.
Mishima, O. (1996). *Nature (London)*, **384**, 546–549.
Mishima, O. & Stanley, H. E. (1998). *Nature (London)*, **396**, 329–335.
Poole, P. H., Essmann, U., Sciortino, F. & Stanley, H. E. (1993). *Phys. Rev. E*, **48**, 4605–4610.
Schober, H., Koza, M., Tölle, A., Fujara, F., Angell, C. A. & Böhmer, R. (1998). *Physica B*, **241–243**, 897–902.
Schober, H., Koza, M. M., Tölle, A., Masciovecchio, C., Sette, F. & Fujara, F. (2000). *Phys. Rev. Lett.* **85**, 4100–4103.
Senker, J., Sehnert, J. & Cornell, S. (2005). *J. Am. Chem. Soc.* **127**, 337–349.
Stanley, H. E., Buldyrev, S. V., Canpolat, M., Mishima, O., Sadr-Lahijanin, M. R., Scala, A. & Starr, F. W. (2000). *Phys. Chem. Chem. Phys.* **2**, 1551–1558.
Tanaka, H. (2000). *Europhys. Lett.* **50**, 340–346.